



Neuronal basis of contrast discrimination

Geoffrey M. Boynton^a, Jonathan B. Demb^a, Gary H. Glover^b, David J. Heeger^{a,*}

^a Department of Psychology, Stanford University, Stanford, CA 94305, USA

^b Department of Diagnostic Radiology, Stanford University, Stanford, CA 94305, USA

Received 17 November 1997; received in revised form 24 March 1998

Abstract

Psychophysical contrast increment thresholds were compared with neuronal responses, inferred from functional magnetic resonance imaging (fMRI) to test the hypothesis that contrast discrimination judgements are limited by neuronal signals in early visual cortical areas. fMRI was used to measure human brain activity as a function of stimulus contrast, in each of several identifiable visual cortical areas. Contrast increment thresholds were measured for the same stimuli across a range of baseline contrasts using a temporal 2AFC paradigm. fMRI responses and psychophysical measurements were compared by assuming that: (1) fMRI responses are proportional to local average neuronal activity; (2) subjects choose the stimulus interval that evoked the greater average neuronal activity; and (3) variability in the observer's psychophysical judgements was due to additive (IID) noise. With these assumptions, fMRI responses in visual areas V1, V2d, V3d and V3A were found to be consistent with the psychophysical judgements, i.e. a contrast increment was detected when the fMRI responses in each of these brain areas increased by a criterion amount. Thus, the pooled activity of large numbers of neurons can reasonably well predict behavioral performance. The data also suggest that contrast gain in early visual cortex depends systematically on spatial frequency. © 1998 Elsevier Science Ltd. All rights reserved.

Keywords: fMRI; Psychophysics; Contrast; Primary visual cortex; Masking

1. Introduction

For more than 30 years, psychophysical studies of visual pattern perception have paralleled research on the neurophysiological response properties of neurons in the visual cortex. The prevailing view has been that psychophysical judgements about pattern discrimination and pattern appearance are limited by neuronal signals in early visual cortical areas (e.g. V1). The response properties of the underlying neuronal mechanisms have been estimated by fitting models of neuronal processing to the psychophysical measurements (Graham, 1989).

We aimed to establish a firmer link between pattern discrimination and neurophysiology. Specifically, we used functional magnetic resonance imaging (fMRI) to measure brain activity as a function of stimulus contrast, while subjects made contrast discrimination judgements. Our results demonstrate that neuronal sig-

nals appropriate for limiting contrast discrimination performance are indeed present as early as V1.

Contrast discrimination thresholds are measured by finding the increment in stimulus contrast that can be reliably detected above some baseline contrast. The increment threshold as a function of baseline contrast, called a threshold versus contrast or TvC function, forms a 'dipper shape'. The contrast increment above a zero baseline contrast is called the absolute threshold. As the baseline contrast increases above zero, the increment threshold drops below the absolute threshold. This effect is called negative masking, facilitation, or the pedestal effect (Nachmias & Sansbury, 1974; Stromeyer & Klein, 1974; Tolhurst & Barfield, 1977; Legge & Foley, 1980). As the baseline contrast increases beyond the range of facilitation, the increment threshold increases well above the absolute threshold. This increase in increment thresholds for high baseline contrasts is called masking.

A popular class of models predict the form of the TvC function by postulating an underlying neuronal contrast–response function that forms an S-shaped

* Corresponding author. Tel: +1 650 7234048; fax: +1 650 7255699; e-mail: heeger@stanford.edu.

nonlinearity. According to these models an increment in contrast can be detected only when the increment in the neuronal response increases by some criterion amount (Legge & Foley, 1980; Foley & Yang, 1991; Foley, 1994; Foley & Boynton, 1994; Teo & Heeger, 1994, 1995). The shape of the TvC function is therefore a simple consequence of the shape of the neuronal contrast–response function; increment thresholds are inversely related to the slope of the neuronal contrast–response function. The expansive portion of the nonlinearity at low contrasts predicts the facilitation effect, while the compressive nonlinearity at high contrasts predicts the masking effect.

Typical V1 neurons show an S-shaped monotonic contrast–response function. That is, with increasing contrast, the neuronal response is expansive at low contrasts and then compressive for higher contrasts (Dean, 1981b; Albrecht & Hamilton, 1982; Sclar, Maunsell & Lennie, 1990; Carandini, Heeger & Movshon, 1997). Thus, area V1 is a natural place to search for the neuronal correlate of contrast increment thresholds.

We tested whether contrast discrimination thresholds are consistent with fMRI contrast–response measurements. In the psychophysical experiments, each trial consisted of two stimulus intervals; a baseline contrast was shown in one interval and a slightly higher contrast was shown in the other interval. Observers chose the interval which appeared to have higher contrast. The contrast increment was adjusted from trial to trial, until it was just barely detectable. In the fMRI experiments, we measured response as a function of stimulus contrast for the same stimuli.

We made three assumptions about how neuronal activity is pooled to yield psychophysical and fMRI responses. First, we assumed that the fMRI responses are proportional to the local average neuronal activity. Second, we assumed that the observers' psychophysical decision rule was to choose the stimulus interval that evoked the greater average neuronal activity. Third, we assumed that the variability in the observer's psychophysical judgements was due to additive, independent and identically distributed (IID) noise. With these assumptions, we can establish a direct link between fMRI responses and psychophysical responses. In particular, the contrast increment should be detected when the fMRI responses (in the appropriate brain area) increase by a criterion amount.

2. Methods

Blood oxygenation level-dependent (BOLD) functional magnetic resonance imaging (Kwong, Belliveau, Chesler, Goldberg, Weiskoff, Poncelet et al., 1992;

Ogawa, Lee, Kay & Tank, 1990; Ogawa, Tank, Menon, Ellermann, Kim, Merkle et al., 1992; Moseley & Glover, 1995) was used to measure brain activity in response to visual stimuli. Each subject participated in several scanning sessions: one to obtain a standard, high-resolution, anatomical scan, one to define the early visual areas including V1, and at least four to measure fMRI contrast–response functions. Psychophysical contrast increment thresholds (TvC curves) were measured in separate sessions.

2.1. Subjects

Two of the authors (gmb and djh) served as subjects for these experiments. Both subjects have normal acuity and are experienced psychophysical observers. The same two subjects served in both behavioral and in imaging experiments to allow a direct comparison between behavioral and brain measurements.

2.2. Visual stimuli

Stimuli were contrast-reversing (8 Hz) plaids (sums of orthogonal sine wave gratings) of either 0.5 or 2 cycles/°, restricted to a peripheral annulus (inner radius, 5°; outer radius, 7°) of the visual field. The mean luminance was 36 cd/m². Stimulus contrast was defined in the usual way as the peak luminance of the stimulus minus the minimum luminance, divided by twice the mean. Restricting the stimulus to a limited range of eccentricities was important because psychophysical contrast thresholds (Robson & Graham, 1981) and the preferred spatial frequencies of cortical neurons (DeValois, Albrecht & Thorell, 1982) both depend on eccentricity. We chose a peripheral annulus rather than a central disk of eccentricities because it is difficult to identify the boundaries between the cortical visual areas for the central part of the visual field.

Visual stimuli were displayed on a screen, made of rear-projection material, positioned 127 cm away from the viewer at the opening of the bore of the magnet near the subject's knees. The stimuli were generated on a Macintosh computer that transmitted a high resolution RGB signal to a Sanyo PLC300M LCD video projector (66.7 Hz refresh). A special purpose lens focused the image on the projection screen.

The subject, lying on his back, looked directly up into an angled mirror to see the rear-projection screen. The display subtended 14 × 14° of visual angle. A small high contrast square in the center of the stimulus served as a fixation mark to minimize effects of eye movements. A bite bar was used to stabilize the subject's head.

2.3. Functional MRI data acquisition

fMRI contrast–response functions were measured for each of two spatial frequencies (0.5 and 2.0 c/°) and at each of six baseline contrasts. Responses to each of the 12 stimulus conditions (six contrasts, two spatial frequencies) were measured in separate scans, and each measurement was repeated two or three times on each of the two subjects.

Each scan lasted 254 s. Visual stimuli were presented and subjects' responses were recorded during a series of test periods (see below), each of which lasted 18 s. The test periods alternated seven times (once every 36 s) with blank periods. A uniform gray field (36 cd/m², equal to the mean luminance of the test stimuli) was presented during these blank periods. The first test/blank cycle (i.e. the first 36 s) of data were discarded to minimize effects of magnetic saturation and visual adaptation. During the remaining 216 s of each scan, a sequence of 72 functional images (one every 3 s) was recorded for each of eight slices through the occipital lobe of the brain.

Subjects performed a contrast discrimination task throughout each of the test periods. Specifically, each 18 s test period consisted of nine trials (2 s each). During each trial, two 0.5 s stimuli (one slightly higher contrast than the other) were presented, separated by a brief blank interval, and followed by a response interval. Subjects indicated which stimulus appeared to have the higher contrast by pressing one of two keys on a response pad specially modified for use in the MR scanner (Resonance Technologies, Northridge, CA).

The two stimulus contrasts were fixed for each 254 s scan. The contrast increment was chosen based on separate psychophysical measurements (see below) so that the subjects would perform with an accuracy of approximately 79% correct. Having the subjects perform the discrimination task in this way during the scan helped to control for their 'attentional state'. Visual feedback ('yes', 'no', or 'XXX' for no response) was displayed just below the fixation point after each response to keep the subjects motivated. A uniform gray field was presented during both the blank and response intervals. Alternating brief stimulus presentations with blank intervals in this way also minimized any effects of contrast–dependent adaptation by visual neurons.

Imaging was performed on a standard clinical GE 1.5 T Signa scanner with a 5 inch diameter surface coil placed at the back of the head. We used a T2*-sensitive gradient recalled echo pulse sequence with a spiral readout (Noll, Cohen, Meyer & Schneider, 1995; Glover & Lai, 1998). Parameters for the protocol were: 1500 TR (repetition time), 40 ms TE (echo time), 90° FA (flip angle), 2 interleaves, inplane resolution = 1.02 × 1.02mm, slice thickness = 4mm. In all experiments, eight adjacent planes of fMRI data were

collected in a pseudo-coronal orientation perpendicular to the calcarine sulcus with the lowest slice near the occipital pole. Structural images were acquired in the same slices as the functional images using a T1-weighted spin echo pulse sequence (500 ms TR, minimum TE, 90 FA) at the same resolution as the functional scans. These inplane anatomical images were registered to a high-resolution, anatomical MRI scan of the subject's brain so that all of the fMRI data from a given subject were aligned to a common three-dimensional coordinate frame.

2.4. Functional MRI data analysis

The fMRI process produces a 256 × 256 × 8 volume of data every 3 s. For a given fMRI voxel (sample point in the 256 × 256 × 8 volume), the image intensity comprises a time-series of data. This time-series was periodic with a period equal to the 36 s stimulus temporal period. We calculated the average amplitude and temporal phase of the fMRI time-series for a given condition by: (1) removing any linear trend in the time-series; (2) dividing each voxel's time-series by the voxel's mean intensity; (3) selecting a set of voxels corresponding to a particular brain region, (e.g. V1, see below); and then (4) calculating the amplitude and phase of the (36 s period) sinusoid that best fit the time-series for each voxel.

To improve signal-to-noise in the contrast–response measurements, the least responsive voxels (e.g. those that contained a high proportion of white matter or those that did not correspond to the 5–7° stimulus annulus) were removed based on a reference scan that was run as the first scan at the beginning of each session. The reference stimulus was a contrast-reversing 8.3 Hz, 1 cycle/° checkerboard restricted to the same 5–7° annulus. This stimulus was alternated every 36 s with a mid-gray field of equal mean luminance. Voxels with correlations above a liberal threshold ($r > 0.23$ with 0–9 s time lag) were included in further analyses. This correlation threshold of $r > 0.23$ corresponds to a $P < 0.025$ (one-tailed) significance level with $n = 72$ given that the 72 points in the time series are independent. The independence assumption is obviously violated in an fMRI time series due to the sluggishness of the hemodynamic response, and so the threshold would have to be raised considerably to achieve the desired significance level. However, this threshold was chosen only to remove the least responsive voxels from the analysis, not to test whether the stimulus was evoking activity.

The final fMRI response was calculated by combining the amplitudes and phases from the remaining voxels. First, we computed the vector mean across these voxels. Secondly, for each subject, the responses to the reference scans were averaged across scanning

sessions to obtain the average reference phase. Finally, the fMRI response was calculated by projecting the vector mean onto a unit vector with the average reference phase. Assuming that the noise in our measurements has random phase, the resulting fMRI response is an unbiased estimate of the true (noise-free) response amplitude, and its probability distribution is unimodal and symmetric.

The S.D. of the random-phase noise in the fMRI responses was estimated separately for each scan. Because the noise in the fMRI images was highly correlated in adjacent voxels, it would have been incorrect to simply compute the S.D. of the responses across voxels and divide by the square root of the number of voxels. Instead, we noted that the Fourier amplitude spectrum of the time series was a smooth function of frequency, and we used the components that were not driven by the stimulus to estimate the noise in the stimulus-driven responses. Fig. 1A, for example, plots the time series (averaged within V1) in response to a 50% contrast stimulus. Fig. 1B plots the amplitude of the Fourier

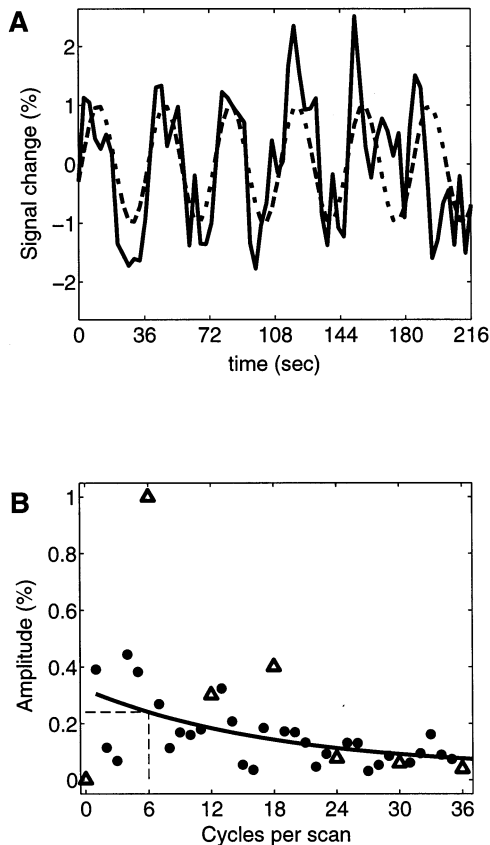


Fig. 1. Response variability. (A) Time series averaged within V1 from subject djh for a 50% contrast stimulus, superimposed with the best fitting sinusoid (dashed line). (B) Amplitude of the Fourier transform of (A). The signal frequency (6 cycles/scan) and its harmonics are represented by triangles. Filled circles correspond to nonharmonic frequencies. Smooth curve is an exponential function fit that was used to estimate the noise amplitude at the signal frequency (dashed line).

transform of this time series. Triangles correspond to the (6 cycles/scan) signal frequency along with its higher harmonics (integer multiples of 6 cycles/scan). An exponential function was fit to the other (nonharmonic) frequency components (filled circles), and as illustrated in Fig. 1B, the fitted value at the signal frequency was used to estimate response variability (σ_i in Eq. (2) below). Assuming again that the noise in our measurements has random phase, the resulting σ_i is an unbiased estimate of the S.D. of the noise.

We believe that the variability in our fMRI measurements is dominated by factors other than neuronal noise for the following four reasons. First, unlike single neurons whose response variance is proportional to the mean response, our noise estimates are largely invariant with respect to the on-harmonic (neuronally driven) signal. Second, our measured noise spectral power distribution is not consistent with that inferred from estimates of the hemodynamic response function (Boynton, Engel, Glover & Heeger, 1996). Third, there are many other potential sources of noise, including hemodynamic response variability and noise in the MR imaging process. Finally, the expected variance of the neuronal noise, after averaging across millions of neurons and over several minutes, should be much smaller than our observed variance.

2.5. Defining visual brain areas

The fMRI data were analyzed separately in each of several retinotopically-organized visual cortical areas (V1, V2v, V2d, V3v, V3d, V3A, and V4v). fMRI methods for defining these areas are now well established (Schneider, Noll & Cohen, 1993; Engel, Rumelhart, Wandell, Lee, Glover, Chichilnisky et al., 1994; Sereno, Dale, reppas, Kwong, Belliveau, Brady et al., 1995; DeYoe, Carman, Bandettini, Glickman, Wieser, Cox et al., 1996; Engel, Glover & Wandell, 1997). The polar angle component of the retinotopic map was measured by recording fMRI responses as a stimulus slowly rotated (like the second hand of a clock) in the visual field. The stimulus was shaped like a wedge that covered 1/8th of the screen, and was filled with contrast-reversing black and white checks (8.4 Hz flicker rate). The stimulus evoked a traveling wave of neuronal activity in the retinotopically-organized visual brain areas. In early visual areas, reversals in the polar angle dimension of the retinotopic layout occur at the area boundaries. For example, as one moves an electrode through a monkey brain from central V1 towards the V2 border, the receptive field centers change from the horizontal towards the vertical meridian. As one crosses the border from V1 and continues into V2, the receptive field centers move from the vertical meridian back towards the horizontal meridian. Similar reversals occur at the V2/V3, V3d/V3A, and V3v/V4v borders

(VanEssen, Felleman, DeYoe, Olavarria & Knierim, 1990). The radial component of the retinotopic map was likewise measured by recording fMRI responses as a ring stimulus (covering 1/8th of the screen, and filled with contrast-reversing checks) slowly expanded from the fixation point into the periphery.

To visualize these retinotopy measurements, a high-resolution MRI of each subject's brain was computationally flattened. First, the gray matter was identified from a high-resolution, anatomical MRI scan, using a Bayesian classification algorithm (Teo, Sapiro & Wandell, 1997). Second, a multidimensional scaling algorithm was used to flatten the cortical sheet (Engel, Glover & Wandell, 1997). The software for segmenting the gray matter and for flattening the cortical surface are available on the World Wide Web at <http://white.stanford.edu>. Third, the retinotopy measurements were projected into the flattened representation. Fourth, the locations of visual area boundaries were drawn by hand on the flattened representation along the reversals in the polar angle (rotating wedge) component of the retinotopic map, and orthogonal to the radial (expanding ring) component of the retinotopic map. The locations of the boundaries can be determined reliably in this way, across repeated experiments, to within an error of 2–4 mm (Engel, Glover & Wandell, 1997). We tried to be conservative in this process and select the areas slightly within the area boundaries. Finally, the selected areas were projected back to three-dimensional coordinates within the gray matter of the brain.

These procedures to define the various visual brain areas were performed only once per subject. Because the fMRI data recorded during successive scanning sessions were all aligned to a common three-dimensional coordinate frame (see above), we could localize the previously labeled visual areas across scanning sessions.

2.6. Psychophysical methods

Psychophysical contrast increment thresholds were measured in separate sessions prior to the fMRI experiments. To ensure that the stimulus conditions were identical for both the psychophysical and fMRI experiments, we used the same peripheral plaid stimuli displayed in the same way with the subjects lying in the MR scanner.

Contrast increment thresholds were measured for each of the two spatial frequencies, and at each of four or five baseline contrasts, using a two-interval forced choice design. As in the fMRI experiments, each trial consisted of two 1/2 s stimulus presentations (a baseline stimulus, and a test stimulus of slightly higher contrast than the baseline), that were separated by a brief blank interval, and followed by a response interval. Subjects

indicated which stimulus appeared to have the higher contrast by pressing one of two keys on a response pad. A uniform gray field was presented during both the blank and response intervals, the fixation point flashed briefly before each stimulus presentation, and visual feedback was provided after each response. Subjects were allowed to take as much time as they desired to respond, although typically they responded at about the same pace as in the fMRI experiments.

The contrast of the test stimulus was adjusted, from trial to trial, using a double random staircase procedure. After three correct responses in a given staircase the test contrast was decreased (i.e. moved closer to that of the baseline stimulus) making the task more difficult. After one incorrect response, the test contrast was increased making the task easier. The two staircases were randomly interleaved and contained a total of 50 trials.

The resulting psychometric function was fit with a Weibull function using a maximum likelihood fitting procedure (Watson, 1979). The contrast increment threshold was defined as the contrast that yielded 79% correct performance, that is the performance level to which the 3-down, 1-up staircase converges. We report the mean of three repeats of each condition. We quantified the variability in the psychophysical data as the S.E. of the mean of the three repeats, rather than using the individual psychometric functions, because we were primarily concerned with reliability across repeated measures given that the fMRI data that were collected in separate experimental sessions.

2.7. Comparing fMRI and psychophysical measurements

fMRI contrast–response functions were fit using the following equation:

$$\hat{R}(C) = a \frac{C^{p+q}}{C^q + \sigma^q} \quad (1)$$

where R is response and C is stimulus contrast. The other symbols determine the shape of the contrast–response function. A typical contrast–response function is shown in Fig. 2A. When $C \gg \sigma$, the function behaves like a simple power function with an exponent of p . When $C \ll \sigma$, the function behaves like a power function with an exponent of $p+q$. Typical values of p and q are 0.3 and 2, respectively, so that the function is expansive ($C^{2.3}$) at low contrasts and compressive ($C^{0.3}$) at high contrasts.

The function in Eq. (1) was fit to the fMRI data by performing a numerical search to minimize the following weighted least-squares error function:

$$\chi^2 = \sum_i \frac{[\hat{R}_i - R_i]^2}{\sigma_i^2} \quad (2)$$

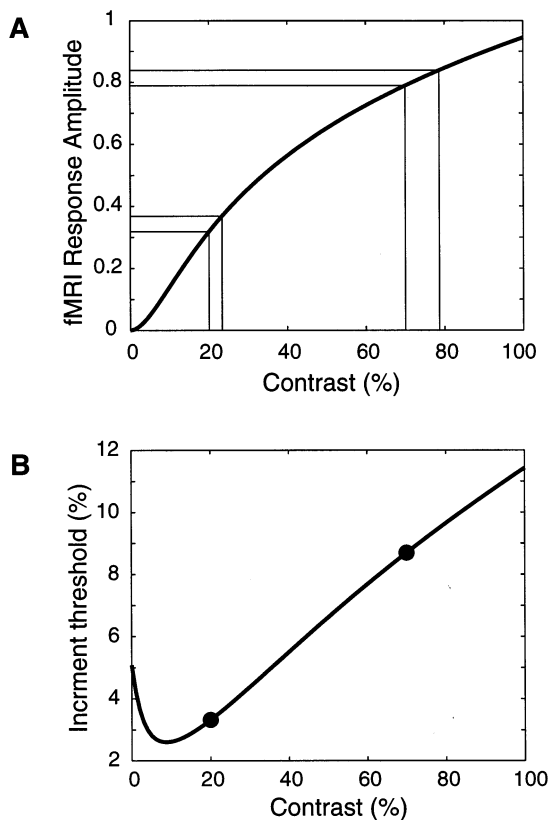


Fig. 2. Illustration of the link between neuronal contrast–response functions and psychophysical TvC curves. (A) A typical contrast–response function, as given by Eq. (1) with parameters: $a=1.0$; $p=0.40$; $q=1.5$; $\sigma=15$. (B) TvC curve predicted from the contrast–response function in (A) according to Eq. (3) with $\Delta R=0.05$. The thin lines in (A) and the filled circles in (B) illustrate an example of the relationship between the two curves (see text).

where R_i is the measured response to the i th scan and \hat{R}_i is the predicted response for that stimulus condition. The responses for each stimulus condition were measured repeatedly (two to three times); each repeat contributed separately to the summation in the error function. The σ_i^2 in the denominator is an estimate of variance of the response (see above), and was included for two reasons. First, the predicted responses would most closely match data points with the smallest estimated variance. Second, by compensating for the relative variability in the two (fMRI and psychophysical) data sets, the fits to each data set could be compared on equal footing (see below).

Psychophysical contrast increment thresholds can be predicted from a contrast–response function (Eq. (1)) by assuming that a contrast increment is detectable when the response increases by a criterion amount (see Introduction). That is, the predicted threshold, ΔC , satisfies:

$$\hat{R}(C + \Delta C) - \hat{R}(C) = \Delta R, \quad (3)$$

where ΔC is the threshold contrast increment and ΔR is the criterion response increment. Eq. (3) can be solved numerically for a variety of baseline contrasts (C) to produce a predicted TvC curve.

Fig. 2 B plots a TvC curve predicted from the contrast–response function in Fig. 2A, according to Eq. (3), with $\Delta R=0.05$. The thin lines in Fig. 2A and the filled circles in Fig. 2B illustrate examples of the relationship between the two curves. For baseline contrasts of 20 and 70%, the contrast increments must be about 3 and 9%, respectively, to evoke the criterion response increment.

The relationship between the contrast–response function plotted in Fig. 2A and the TvC curve plotted in Fig. 2 B can be approximated by noting that:

$$\frac{dR}{dC} \approx \frac{\Delta R}{\Delta C} \quad (4)$$

Hence the TvC curve is approximately proportional to 1 over the derivative of the contrast–response function:

$$\Delta C \approx \Delta R \frac{1}{dR/dC} \quad (5)$$

The relative values of σ , p , and q determine the shape of the TvC curve and the criterion response, ΔR , scales the TvC curve. In particular, the predicted contrast thresholds increase with baseline contrast for high contrasts ($C \gg \sigma$) where the contrast–response function is compressive. At low contrasts ($C \ll \sigma$) where the contrast–response function is expansive, on the other hand, the predicted contrast thresholds decrease with increases in baseline contrast. Changing ΔR shifts the curve vertically on the log scale, e.g. doubling ΔR will roughly double the contrast thresholds according to Eq. (5). For a fixed value of ΔR , the absolute threshold (at zero baseline contrast) is determined by σ .

Predicted TvC curves were fit to the psychophysical data using Eq. (2), as described above. Simultaneous fits to the fMRI and psychophysical data were performed by minimizing the sum of the respective errors; dividing by the variance in the denominator (Eq. (2)) compensated for the relative variability in the two data sets.

3. Results

3.1. Contrast–response functions in V1

Fig. 3A and 3B plot fMRI responses as a function of stimulus contrast for visual area V1 in subject djh. The two graphs correspond to the two different spatial frequencies. The smooth curves are the simultaneous fit to both fMRI and psychophysical data (see below). Each data point is the result of a single scan. The results in Fig. 3 A,B illustrate the reliability of our

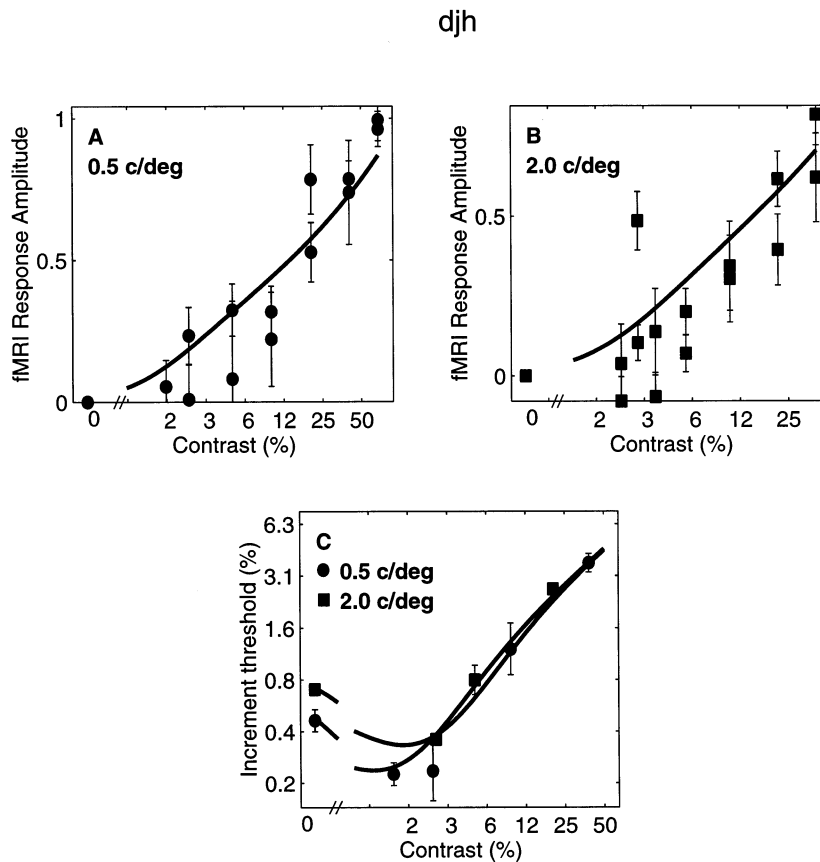


Fig. 3. (A) and (B) fMRI responses for subject djh in visual area V1 as a function of stimulus contrast at 0.5 c/° and 2.0 c/°, respectively. Each data point is the result of a single scan. Two slightly different contrasts were displayed during the test periods of each scan (see Methods). The x-axis value of each data point is plotted at the average of these two contrasts. (C) Psychophysical TvC data at the same two spatial frequencies. Smooth curves were fit to both fMRI and psychophysical data, simultaneously at both spatial frequencies.

measurements. The two repeats of each stimulus condition, collected in separate scanning sessions, usually give very nearly the same response to within the estimated measurement error indicated by the error bars (except for one aberrant data point discussed further below). Note that, unlike Fig. 2 A, contrast is plotted on a logarithmic axis.

3.2. Threshold versus contrast (TvC) curves

Fig. 3C plots the psychophysical TvC curves for subject djh. The smooth curves are the simultaneous fit to both fMRI responses in V1 and the psychophysical data. The thresholds initially drop at low contrasts and then rise for higher contrasts, forming the familiar ‘dipper function’ commonly reported in masking experiments Nachmias & Sansbury, 1974.

3.3. Comparison of psychophysical and fMRI measurements in V1

The two (fMRI and psychophysics) data sets, including results from both spatial frequencies, were fit simul-

taneously using a total of six parameters. Fits to both spatial frequencies shared the common parameters from Eq. (1) of σ , p , and q . Two values of sigma, $\sigma_{0.5}$ and $\sigma_{2.0}$, were allowed to differ for the two spatial frequencies. Finally, a single criterion response value, ΔR , allowed increment thresholds to be predicted from contrast–response functions using Eq. (3). The fits are impressive (smooth curves pass through nearly all of the error bars), i.e. the fMRI and psychophysical data agree.

Fig. 4 shows results for the second subject, gmb. Fig. 4A,B plot the fMRI contrast–response data from V1 and Fig. 4C plots the psychophysical TvC data. The smooth curves are again a simultaneous fit to both the fMRI and the psychophysics, at both spatial frequencies. The fits for this second subject are also reasonably good; the model predictions pass through most of the error bars.

Parameter values for the best simultaneous fits for subjects djh and gmb are provided in Tables 1 and 2, respectively. The best-fit exponents (that relate the slopes of the two curves) are the critical parameters that make the two data sets agree. Masking typically occurs

gmb

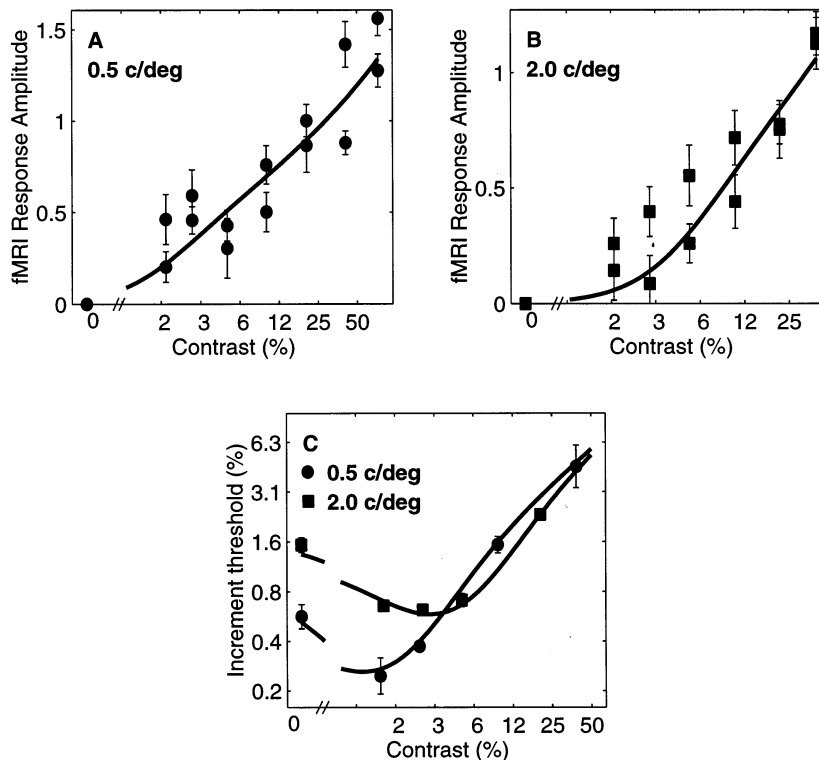


Fig. 4. fMRI responses in V1 and TvC data for subject gmb (same format as Fig. 3).

only for background contrasts well above detection threshold. In this regime, the contrast increment thresholds increase with background contrast as a power function, with an exponent of about 0.5–0.7 (Legge & Foley, 1980; Legge, 1981). This implies an exponent of 0.3–0.5 in the underlying neuronal contrast–response functions. Our best-fit parameter values likewise imply a power function masking regime when $C \gg \sigma$ with $p \approx 0.3$. Facilitation typically occurs only for low background contrasts. Psychophysically-based estimates of the underlying neuronal contrast–response function suggest an expansive regime with an exponent of about 2.5–2.7 (Foley, 1994). Our best-fit parameter values likewise imply an expansive facilitation regime when $C \ll \sigma$ with $p + q \approx 1.6$; the difference between this number and previous results may be due to the various methodological differences (e.g. stimulus size, temporal frequency etc.).

The best-fit parameter values of ΔR are ~ 0.03 , meaning that two stimuli producing fMRI responses that differ by this amount will be distinguishable by an observer approximately 79% of the time, regardless of the baseline contrast.

To further test the correspondence between V1 neuronal activity and psychophysical performance, we determined the best-fitting parameter values to Eq. (1)

separately for the fMRI data and the psychophysical data. These values for subjects djh and gmb are provided in Tables 3 and 4, respectively. The values of the p and q parameter estimates are similar across the two experiments. There is less agreement in the σ parameters across experiments.

A statistical bootstrapping procedure (Efron & Tibshirani, 1993) was used to test if there was a significant difference between the parameter values fit to the two (fMRI and psychophysics) data sets. The procedure consisted of three steps: (1) randomly sample values from the Gaussian distributions defined by the means and standard deviations of the responses to each contrast level; (2) fit the resampled data with Eq. (1); and (3) record the fitted parameter values. These three steps were repeated 200 times to generate bootstrapped probability distributions of the parameter values. Fig. 5 plots the bootstrapped distributions from the fMRI data (X's) superimposed with the bootstrapped distributions from the psychophysical data (filled O's). The distributions for the p and q parameters largely overlap, i.e. the parameter values estimated from two data sets (fMRI and psychophysics) are consistent with one another. The bootstrapped distributions for the σ parameters do not overlap substantially. However, we suspect that the fMRI data may not have constrained

Table 1
Parameter values fit jointly to psychophysical and fMRI data for subject djh

Area	a	$\sigma_{0.5}$	$\sigma_{2.0}$	p	q	ΔR	x^2 Tvc	x^2 fMRI	Total x^2
V1	0.99	1.55	2.58	0.33	1.55	0.02	9.22	74.86	84.08
V2d	0.82	1.53	2.31	0.34	1.62	0.02	7.18	58.30	65.49
V3d	0.67	1.47	2.35	0.31	1.66	0.02	3.89	57.83	61.73
V3A	0.48	0.60	1.23	0.22	5.19	0.01	8.41	80.46	88.88

these parameters particularly well because they are determined primarily by the responses at the lowest contrasts. This suspicion is reinforced by the fact that many of the fMRI-bootstrapped σ values equal zero, the lower bound allowed by the fitting procedure.

There is one aberrant data point in subject djh's contrast–response function at 2 c/° (Fig. 3B) at a contrast of around 3% which is clearly much higher than neighboring points. A re-analysis of the simultaneous fits without this data point shows a better goodness of fit but the parameter values do not change substantially, and hence our conclusions do not change.

3.4. Facilitation

Contrast discrimination thresholds decrease below absolute threshold for low baseline contrasts. There are two models that can predict this facilitation effect. The model that we have adopted in Eqs. (1) and (3) predicts facilitation through a combination of: (1) an expansive contrast–response function, and (2) the assumption that equal differences in responses are equally discriminable across the entire range of contrasts. The second model is that of Pelli (1985), the uncertainty model which assumes a psychophysical decision rule based on the maximum of the responses of each individual neuron to each of the two stimuli. For stimuli near absolute threshold, the maximum response may come (by chance, due to noise) from any of a very large number of neurons. Most of these neurons are not driven by the stimuli because they have inappropriate receptive fields or because they are tuned for inappropriate spatial frequencies, orientations, etc. They thus contribute only noise to the decision. Once above absolute threshold, the maximum response may come only from those neurons that are driven by the stimulus, and hence the

noise is reduced. Both models can predict facilitation at low contrasts equally well (Pelli, 1985).

To test which of these explanations is correct, we looked for an expansive regime in the contrast–response functions at low contrasts. The best-fit values of $p + q$ from the fMRI data are 1.8 and 1.36 for subjects djh and gmb, respectively (see Tables 3 and 4). These values are greater than 1, consistent with an expansive nonlinearity at low contrasts. In fact, the values of the p and q parameter estimates are quite similar across the two (fMRI and psychophysics) experiments (see above), again consistent with the expansive nonlinearity hypothesis.

We used the bootstrapped distributions of the p and q parameter values to evaluate the statistical significance of the evidence for an expansive nonlinearity. The dashed lines in Fig. 5 A,B indicate $p + q = 1$. Parameter values estimated from the fMRI data are indicated by the X's. Points below the line represent parameter values that are inconsistent with an expansive nonlinearity. Two of the 200 points lie below the line for subject djh, while 55 of the 200 points lie below the line for subject gmb. Hence, the evidence for an expansive nonlinearity is statistically significant in only one of the two subjects. Further repeats of the measurements might be used to disambiguate these results.

3.5. Effect of spatial frequency

Contrast detection thresholds depend on spatial frequency (Graham, 1989). Detection judgements depend inherently on both the strength of the signal and the level of the internal noise. There are, therefore, two mechanisms that might underlie the spatial frequency dependence of contrast sensitivity. First, contrast gain in some visual area(s) might depend systematically on

Table 2
Parameter values fit jointly to psychophysical and fMRI data for subject gmb

Area	a	$\sigma_{0.5}$	$\sigma_{2.0}$	p	q	ΔR	x^2 TvC	x^2 fMRI	Total x^2
V1	1.48	1.64	5.21	0.30	1.58	0.04	5.32	64.41	69.73
V2d	0.99	1.67	5.25	0.30	1.52	0.03	6.19	68.12	74.30
V3d	1.08	1.68	4.67	0.33	1.66	0.03	6.83	92.03	98.86
V3A	0.68	1.76	5.11	0.31	1.61	0.02	5.09	72.33	77.42

Table 3

Parameter values fit separately to psychophysical and fMRI data for subject djh

	a	$\sigma_{0.5}$	$\sigma_{2.0}$	p	q	Total χ^2
Psychophysics	—	1.22	1.90	0.34	1.86	2.94
V1 fMRI	1.16	2.56	6.96	0.40	1.40	44.38

spatial frequency. Second, the internal noise might depend systematically on spatial frequency, e.g. as suggested by Brady and Field (1995).

The model that we have used to fit our data can encompass both of these possibilities. Different gains across spatial frequencies corresponds to letting the σ parameter vary with spatial frequency, as in the joint fits described above. Spatial frequency dependent noise corresponds to letting the ΔR parameter vary across spatial frequency. Changing ΔR would produce a vertical shift of the TvC curves. It is clear from the psychophysical data in Fig. 3C and Fig. 4C that the curves shift horizontally as well vertically so that they lie on top of one another in the masking regime at high background contrasts (Bradley & Ohzawa, 1986). This is consistent with a change of gain across spatial frequencies, but not with spatial frequency dependent noise.

To further test which of these two explanations is correct, we looked for a difference in the contrast gains of our fMRI measurements across the two spatial frequencies. If the contrast gain hypothesis is correct, then the $\sigma_{2.0}$ parameter should be significantly larger than the $\sigma_{0.5}$ parameter. As listed in Tables 3 and 4, the best-fit parameter values follow this trend, $\sigma_{2.0} > \sigma_{0.5}$. The statistical significance of this difference was evaluated by comparing the bootstrapped distributions of the two σ values. This trend was statistically significant ($P < 0.01$) for both subjects.

3.6. Other visual areas

Reliable fMRI responses were obtained from three other visual areas: V2d, V3d, and V3A. Contrast–response functions from the ventral visual areas, V2v, V3v and V4v were highly variable across repeated measurements and often non-monotonic. We believe that this may be because the ventral areas were further

Table 4

Parameter values fit separately to psychophysical and fMRI data for subject gmb

	a	$\sigma_{0.5}$	$\sigma_{2.0}$	p	q	Total χ^2
Psychophysics	—	1.89	5.51	0.29	1.57	4.63
V1 fMRI	1.57	0.01	1.17	0.39	0.97	52.37

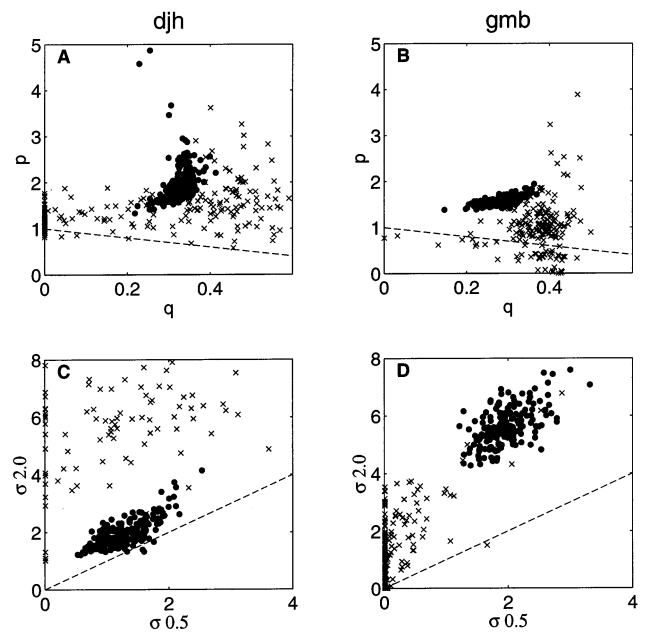


Fig. 5. Scatter plots of bootstrapped parameter values estimated from fMRI data (X symbols) superimposed on bootstrapped parameter values from psychophysics (filled O symbols) (A) and (B), bootstrapped distributions of p and q parameters for the two subjects. Dashed lines indicate $p + q = 1$. (C) and (D), bootstrapped distributions of $\sigma_{2.0}$ and $\sigma_{0.5}$ parameters. Dashed lines indicate $(\sigma_{2.0} = \sigma_{0.5})$.

from the surface coil, so signals from these areas suffered poor signal-to-noise relative to the dorsal visual areas.

For the dorsal areas, parameter values from the best simultaneous fits for both subjects are provided in Tables 1 and 2. The best-fit parameter values do not vary greatly or systematically across these visual areas, which indicates that neuronal contrast–response functions are similar in these areas. Also, there are no systematic differences in goodness of fit across the visual areas.

We do not report parameter values from independently fitting the fMRI data outside V1, because the data did not sufficiently constrain the model in those visual areas.

Not all brain areas have response properties that are consistent with the psychophysical data. Several lines of evidence suggest that a lateral region of the occipital lobe of the human brain, that we refer to as the human MT complex, may be homologous to monkey MT along with surrounding motion-sensitive visual areas (Zeki, Watson, Lueck, Friston, Kennard & Frackowiak, 1991; Tootell & Taylor, 1995; Tootell, Reppas, Kwong, Malach, Born, Brady et al., 1995). Although our slice prescription did not include the MT complex, we know from previous studies (Tootell, Reppas, Kwong, Malach, Born, Brady et al., 1995; Demb, 1997) that contrast–response functions in this area show extremely high gain at low contrasts and near complete

saturation at high contrasts. Such a contrast–response function would predict unreasonably large contrast increment thresholds at high contrasts that would clearly be inconsistent with the psychophysical data.

4. Discussion

Contrast–response functions in areas V1, V2d, V3d and V3A were found to be consistent with psychophysically measured contrast increment thresholds, at each of the two spatial frequencies tested. This suggests that contrast discrimination judgements are limited by neuronal signals in early visual cortical areas. In particular, facilitation at low contrasts and masking at high contrasts can both be explained by the shapes of the neuronal contrast–response functions that are expansive at low contrasts and compressive at high contrasts.

4.1. Three assumptions for comparing fMRI and psychophysics

The comparison between fMRI responses and psychophysical performance was based on three assumptions. First, we assumed that fMRI responses are proportional to the local average neuronal activity, averaged over a small region of the brain and averaged over a period of time. The sequence of events from neuronal response to fMRI response is complicated and only partially understood. It is unlikely that the complex interactions between neurons, regional blood flow, and the MR scanner would result in a precise averaging of the neuronal responses. Even so, local averaging might be a reasonable approximation of these complex interactions. Indeed, we have performed two empirical tests that support the validity of this approximation (Boynton, Engel, Glover & Heeger, 1996): (1) fMRI responses in human V1 depend separably on stimulus timing and stimulus contrast; and (2) responses to long duration stimuli can be predicted from responses to shorter duration stimuli. Although these results did not prove that fMRI responses are proportional to local average neuronal activity (there could be ‘hidden’ nonlinearities), we could not rule out the local averaging approximation.

The second assumption underlying our comparison between fMRI and psychophysics was to assume that subjects performed each trial of the contrast discrimination task by choosing the stimulus that evoked the greater average neuronal activity. A possible alternative decision rule is that observers monitored the responses of only a subset of neurons (e.g. those that are optimally tuned for the particular stimuli being discriminated) when making psychophysical judgements, at a spatial resolution that is too fine for current fMRI techniques. There is, however, some indirect evidence

that is consistent with our assumed psychophysical decision rule. Shadlen, Britten, Newsome and Movshon (1996), in particular, used numerical simulations to try to understand how neuronal signals in area MT support psychophysical performance in a direction discrimination task. They concluded that the monkeys in their experiments apparently based their psychophysical judgements on signals carried by the average responses of a large population of neurons, including many neurons that were not tuned optimally for the particular stimuli being discriminated.

Third, we adopted a model of the internal noise. We assumed that the variability in the observers’ psychophysical judgements was due to additive, independent, and identically distributed (IID) noise. This is a common assumption in detection/discrimination psychophysics, and it implies that equal steps in internal response (e.g. average neuronal activity) are equally discriminable. We are well aware that the variability in single cell responses is not described by additive IID noise. Rather, the variance in a cortical neuron’s firing rate is proportional to its mean firing rate (Dean, 1981a; Tolhurst, Movshon & Dean, 1983; Bradley, Skottun, Ohzawa, Sclar & Freeman, 1987; Snowden, Treue & Anderson, 1992; Britten, Shadlen, Newsome & Movshon, 1993; Softky & Koch, 1993). However, we assume that performance is limited not by the noise in these early sensory neurons, but rather by noise added at a central decision stage of processing. Indeed, Shadlen, Britten, Newsome and Movshon (1996), relied on additive central noise to reconcile differences between their MT neural data and their direction discrimination psychophysical data.

4.2. The parametric form for the contrast–response function

The particular form of the contrast–response function (Eq. (1)) was chosen because it has been used successfully both to fit psychophysical TvC data (Foley, 1994; Foley & Boynton, 1994; Teo & Heeger, 1994, 1995) and to fit electrophysiological contrast–response data (Bonds, 1989; Albrecht & Geisler, 1991; Heeger, 1991, 1992a,b, 1993; DeAngelis, Robson, Ohzawa & Freeman, 1992; Carandini & Heeger, 1994; Carandini, Heeger & Movshon, 1997; Tolhurst & Heeger, 1997a,b; Nestares & Heeger, 1997). It also has the desirable property of being differentiable and it predicts differentiable TvC functions. It is possible that a different parametric form predicts our results equally well. For example, the contrast–response functions in Figs. 3 and 4 could be predicted by zero response at low contrasts up to some threshold followed by a power function. This would also predict a dipper-shaped TvC function, but with a sharp notch (non-differentiable point) at the minimal threshold. Our goal, however, is not to find an optimal parametric form to fit the data, but to show

that the fMRI and psychophysical results agree when compared using a parametric form that has been used in previous studies of brain and behavior.

4.3. Single unit studies of pattern detection/discrimination

Tolhurst, Movshon and Dean, 1983 and Hawken and Parker (1990) recorded from single neurons in cat and monkey primary visual cortex, and compared the neural responses with behavioral measurements of absolute contrast detection thresholds. They found that behavioral thresholds could indeed be well predicted by from the responses of the most sensitive single neurons.

Barlow, Kaushal, Hawken and Parker (1987) and Geisler and Albrecht (1997) recorded the responses of neurons from the primary visual cortex of cats and monkeys, and used those measurements to predict entire contrast discrimination threshold (TvC) curves. We concentrate here on the Geisler and Albrecht study because it was much more extensive. They found that behavioral contrast discrimination functions were similar in shape to: (1) the envelope of the neuronal discrimination functions of the most sensitive cells, and (2) the contrast discrimination functions obtained by (Bayesian) optimal pooling of the entire population of cells. However, the absolute level of optimally pooled neuronal discriminations was far better than behavioral performance. Geisler and Albrecht showed that the performance using optimal pooling could be degraded to match the behavioral performance by adding an efficiency factor, which suggests that noise is added after the early sensory responses. Our model is similar in spirit; we assume that noise at the central decision dominates the early sensory noise and is the limiting factor in the psychophysical judgements. In addition, there was little or no evidence for facilitation in their optimally pooled neuronal discrimination functions. Our assumed psychophysical decision rule is non-optimal; it simply averages the activities of a large population of neurons, many of which are not optimally tuned for the particular stimuli being discriminated. It would be interesting to reanalyze the Geisler and Albrecht data using this non-optimal neuronal pooling rule in conjunction with some assumption about the covariance of neural responses and additive noise at the central decision stage; perhaps this would provide a better prediction of their behavioral data.

Acknowledgements

Special thanks to B.A. Wandell for generous support and advice. Supported by an NIMH postdoctoral research fellowship (F32-MH10897) to G.M. Boynton; by an NIH National Center for Research Resources grant

(P41-RR09784) to G.H. Glover; and by an NIMH grant (R29-MH50228), a Stanford University Research Incentive Fund grant, and an Alfred P. Sloan Research Fellowship to D.J. Heeger.

References

- Albrecht, D. G., & Geisler, W. S. (1991). Motion sensitivity and the contrast-response function of simple cells in the visual cortex. *Visual Neuroscience*, 7, 531–546.
- Albrecht, D. G., & Hamilton, D. B. (1982). Striate cortex of monkey and cat: Contrast response function. *Journal of Neurophysiology*, 48, 217–237.
- Barlow, H. B., Kaushal, T. P., Hawken, M., & Parker, A. J. (1987). Human contrast discrimination and the threshold of cortical neurons. *Journal of the Optical Society of America A*, 4, 2366–2371.
- Bonds, A. B. (1989). Role of inhibition in the specification of orientation selectivity of cells in the cat striate cortex. *Visual Neuroscience*, 2, 41–55.
- Boynton, G. M., Engel, S. A., Glover, G. H., & Heeger, D. J. (1996). Linear systems analysis of fMRI in human V1. *Journal of Neuroscience*, 16, 4207–4221.
- Bradley, A., & Ohzawa, I. (1986). A comparison of contrast detection and discrimination. *Vision Research*, 26, 991–997.
- Bradley, A., Skottun, B., Ohzawa, I., Sclar, G., & Freeman, R. D. (1987). Visual orientation and spatial frequency discrimination; A comparison of single neurons and behavior. *Journal of Neurophysiology*, 57, 755–772.
- Brady, N., & Field, D. J. (1995). What's constant in contrast constancy? The effects of scaling on the perceived contrast of band-pass patterns. *Vision Research*, 35, 739–756.
- Britten, K. H., Shadlen, M. N., Newsome, W. T., & Movshon, J. A. (1993). Responses of neurons in macaque MT to stochastic motion signals. *Visual Neuroscience*, 10, 1157–1169.
- Carandini, M., & Heeger, D. J. (1994). Summation and division by neurons in primate visual cortex. *Science*, 264, 1333–1336.
- Carandini, M., Heeger, D. J., & Movshon, J. A. (1997). Linearity and normalization of simple cells of the macaque primary visual cortex. *Journal of Neuroscience*, 17, 8621–8644.
- Dean, A. F. (1981a). The variability of discharge of simple cells in the cat striate cortex. *Experimental Brain Research*, 44, 437–440.
- Dean, A. F. (1981b). The relationship between response amplitude and contrast for cat striate cortical neurons. *Journal of Physiology (London)*, 318, 413–427.
- DeAngelis, G. C., Robson, J. G., Ohzawa, I., & Freeman, R. D. (1992). The organization of suppression in receptive fields of neurons in the cat's visual cortex. *Journal of Neurophysiology*, 68, 144–163.
- Demb J.B. Functional magnetic resonance imaging of early visual pathways in dyslexia. PhD thesis, Department of Psychology, Stanford University, 1997.
- DeValois, R. L., Albrecht, D. G., & Thorell, L. G. (1982). Spatial frequency selectivity of cells in macaque visual cortex. *Vision Research*, 21, 545–559.
- DeYoe, E. A., Carman, G. J., Bandettini, P., Glickman, S., Wieser, J., Cox, R., Miller, D., & Neitz, J. (1996). Mapping striate and extrastriate visual areas in human cerebral cortex. *Proceedings of the National Academy of Science*, 93, 2382–2386.
- Efron, B., & Tibshirani, R. J. (1993). *An introduction to the bootstrap*. New York: Chapman and Hall.
- Engel, S. A., Glover, G. H., & Wandell, B. A. (1997). Retinotopic organization in human visual cortex and the spatial precision of functional MRI. *Cerebral Cortex*, 7, 181–192.

- Engel, S. A., Rumelhart, D. E., Wandell, B. A., Lee, A. T., Glover, G. H., Chichilnisky, E. J., & Shadlen, M. N. (1994). fMRI of human visual cortex. *Nature*, *369*, 525.
- Foley, J. M., & Boynton, G. M. (1994). A new model of human luminance pattern vision mechanisms: Analysis of the effects of pattern orientation, spatial phase, and temporal frequency. In T. A. Lawton, *Computational vision based on neurobiology*. SPIE Proceedings, Vol. 2054.
- Foley, J. M., & Yang, Y. (1991). Forward pattern masking; effects of spatial frequency and contrast. *Journal of the Optical Society of America A*, *8*, 2026–2037.
- Foley, J. M. (1994). Human luminance pattern-vision mechanisms; masking experiments require a new model. *Journal of the Optical Society of America A*, *11*, 1710–1719.
- Geisler, W. S., & Albrecht, D. G. (1997). Visual cortex neurons in monkeys and cats: Detection, discrimination and identification. *Visual Neuroscience*, *14*, 897–919.
- Glover, G. H., & Lai, S. (1998). Self-navigating spiral fMRI; Interleaved versus single-shot. *Magnetic Resonance Medicine*, *39*, 361–368.
- Graham, N. (1989). *Visual Pattern Analyzers*. New York: Oxford University Press.
- Hawken, M. J., & Parker, A. J. (1990). Detection and discrimination mechanisms in the striate cortex of the old-world monkey. In C. Blakemore, *Vision: coding and efficiency*. Cambridge: Cambridge University Press, 103–116.
- Heeger, D. J. (1991). Nonlinear model of neural responses in cat visual cortex. In M. Landy, & J. A. Movshon, *Computational models of visual processing*. Cambridge, MA: MIT Press, 119–133.
- Heeger, D. J. (1992a). Normalization of cell responses in cat striate cortex. *Visual Neuroscience*, *9*, 181–198.
- Heeger, D. J. (1992b). Half-squaring in responses of cat simple cells. *Visual Neuroscience*, *9*, 427–443.
- Heeger, D. J. (1993). Modelling simple cell direction selectivity with normalized, half-squared, linear operators. *Journal of Neurophysiology*, *70*, 1885–1898.
- Kwong, K. K., Belliveau, J. W., Chesler, D. A., Goldberg, I. E., Weiskoff, R. M., Poncelet, B. P., Kennedy, D. N., Hoppel, B. E., Cohen, M. S., Turner, R., Cheng, H. M., Brady, T. J., & Rosen, B. R. (1992). Dynamic magnetic resonance imaging of human brain activity during primary sensory stimulation. *Proceedings of the National Academy of Science*, *89*, 5675–5679.
- Legge, G. E., & Foley, J. M. (1980). Contrast masking in human vision. *Journal of the Optical Society of America A*, *70*, 1458–1470.
- Legge, G. E. (1981). A power law for contrast discrimination. *Vision Research*, *21*, 457–467.
- Moseley, M. E., & Glover, G. H. (1995). Functional MR imaging. Capabilities and limitations. *Functional Neuroimaging*, *5*, 161–191.
- Nachmias, J., & Sansbury, R. (1974). Grating contrast; Discrimination may be better than detection. *Vision Research*, *14*, 1039–1042.
- Nestares, O., & Heeger, D. J. (1997). Modelling the apparent frequency specific suppression in simple cells responses. *Vision Research*, *37*, 1535–1543.
- Noll, D., Cohen, J., Meyer, C., & Schneider, W. (1995). Spiral k-space MR imaging of cortical activation. *JMRI*, *5*, 49–57.
- Ogawa, S., Lee, T., Kay, A., & Tank, D. (1990). Brain magnetic resonance imaging with contrast dependent on blood oxygenation. *Proceedings of the National Academy of Science*, *87*, 9868–9872.
- Ogawa, S., Tank, D., Menon, R., Ellerman, J., Kim, S., Merkle, H., & Ugurbil, K. (1992). Intrinsic signal changes accompanying sensory stimulation: Functional brain mapping using MRI. *Proceedings of the National Academy of Science*, *89*, 5951–5955.
- Pelli, D. G. (1985). Uncertainty explains many aspects of visual contrast detection and discrimination. *Journal of the Optical Society of America A*, *2*, 1508–1532.
- Robson, J. G., & Graham, N. (1981). Probability summation and regional variation in contrast sensitivity across the visual field. *Vision Research*, *21*, 409–418.
- Schneider, W., Noll, D. C., & Cohen, J. D. (1993). Functional topographic mapping of the cortical ribbon in human vision with conventional MRI scanners. *Nature*, *365*, 150–153.
- Sclar, G., Maunsell, J. H. R., & Lennie, P. (1990). Coding of image contrast in central visual pathways of the macaque monkey. *Vision Research*, *30*, 1–10.
- Sereno, M. I., Dale, A. M., Reppas, J. B., Kwong, K. K., Belliveau, J. W., Brady, T. J., Rosen, B. R., & Tootell, R. B. H. (1995). Borders of multiple visual areas in humans revealed by functional magnetic resonance imaging. *Science*, *268*, 889–893.
- Shadlen, M. N., Britten, K. H., Newsome, W. T., & Movshon, J. A. (1996). A computational analysis of the relationship between neuronal behavioural responses to visual motion. *Journal of Neuroscience*, *15*, 1486–1510.
- Snowden, R. J., Treue, S., & Anderson, R. A. (1992). The response of neurons in macaque MT of the alert rhesus monkey to moving dot patterns. *Experimental Brain Research*, *88*, 389–400.
- Softky, W. R., & Koch, C. (1993). The highly irregular firing of cortical cells is inconsistent with temporal integration of random EPSPs. *Journal of Neuroscience*, *13*, 334–350.
- Stromeyer, C. F., & Klein, S. (1974). Spatial frequency channels in human vision as asymmetric (edge) mechanisms. *Vision Research*, *14*, 1409–1420.
- Teo P., & Heeger D.J. Perceptual image distortion. In: Proceedings of First International Conference on Image Processing. Austin, TX, 1994: 982–6.
- Teo, P., & Heeger, D. J. (1995). A general mechanistic model of spatial pattern detection. *Investigative Ophthalmology Visual Science Suppl*, *36*, 439.
- Teo, P., Sapiro, G., & Wandell, B. A. (1997). Creating connected representations of cortical gray matter for functional MRI visualization. *IEEE Medical Transactions*, *16*, 852–863.
- Tolhurst, D. J., & Barfield, L. P. (1977). Interactions between spatial frequency channels. *Vision Research*, *18*, 51–58.
- Tolhurst, D. J., & Heeger, D. J. (1997a). Comparison of contrast normalization and threshold models of the responses of simple cells in cat striate cortex. *Visual Neuroscience*, *14*, 293–310.
- Tolhurst, D. J., & Heeger, D. J. (1997b). Contrast normalization and a linear model for the directional selectivity of simple cells in cat striate cortex. *Visual Neuroscience*, *14*, 19–26.
- Tolhurst, D. J., Movshon, J. A., & Dean, A. F. (1983). The statistical reliability of single neurons in cat and monkey visual cortex. *Vision Research*, *23*, 775–785.
- Tootell, R. B. H., & Taylor, J. B. (1995). Anatomical evidence for MT and additional cortical visual areas in humans. *Cerebral Cortex*, *5*, 39–55.
- Tootell, R. B. H., Reppas, J. B., Kwong, K. K., Malach, R., Born, R. T., Brady, T. J., Rosen, B. R., & Belliveau, J. W. (1995). Functional analysis of human MT and related visual cortical areas using magnetic resonance imaging. *Journal of Neuroscience*, *15*, 3215–3230.
- VanEssen, D. C., Felleman, D. J., DeYoe, E. A., Olavarria, J., & Knierim, J. (1990). Modular and hierarchical organization of extrastriate visual cortex in the macaque monkey. *Cold Spring Harbor Symposia on Quantitative Biology*, *55*, 679–696.
- Watson, A. B. (1979). Probability summation over time. *Vision Research*, *19*, 515–522.
- Zeki, S., Watson, J. D. G., Lueck, C. J., Friston, K. J., Kennard, C., & Frackowiak, R. S. (1991). A direct demonstration of functional specialization in human visual cortex. *Journal of Neuroscience*, *11*, 641–649.